

# Constraints on evaporating primordial black holes from the AMS-02 positron data

Jia-Zhi Huang

*Institute of Theoretical Physics, Chinese Academy of Sciences, Beijing 100190, China.  
University of Chinese Academy of Sciences, Beijing, 100190, China.*

Yu-Feng Zhou

*Institute of Theoretical Physics, Chinese Academy of Sciences, Beijing 100190, China.  
University of Chinese Academy of Sciences, Beijing, 100190, China. and*

*School of Fundamental Physics and Mathematical Sciences,  
Hangzhou Institute for Advanced Study, UCAS, Hangzhou 310024,  
China. International Centre for Theoretical Physics Asia-Pacific, Beijing/Hangzhou, China.*

(Dated: March 11, 2024)

## Abstract

Cosmic-ray (CR) positrons are relatively rare due to its secondary origin and thus sensitive to exotic contributions. Primordial black holes (PBHs) with masses above  $\sim 5 \times 10^{14}$  g can be stable sources of CR positrons due to Hawking radiation. We show that the CR positron flux measured by AMS-02 can place stringent constraints on the energy fraction of PBHs relative to that of dark matter  $f_{\text{PBH}}$ . Making use of the state-of-the-art models for CR propagation in both the Galaxy and heliosphere, we obtain conservative upper limit of  $f_{\text{PBH}} \lesssim 3 \times 10^{-4}$  at  $M_{\text{PBH}} \simeq 2 \times 10^{16}$  g, which improves the previous constraints obtained from the Voyager CR all-electron data by around an order of magnitude.

## I. INTRODUCTION

Astrophysical and cosmological observations suggest that the dominant part of the matter in the present Universe is in the form of non-luminous dark matter (DM). In many particle physics models, DM consists of a new type of elementary particle beyond the Standard Model (SM) of particle physics, which may participate non-gravitational interactions with baryonic matter, such as weakly interacting massive particles (WIMPs), sterile neutrinos, QCD axions and ultralight bosonic particles. Despite great experimental efforts in recent decades, so far there is no confirmed signals of particle DM from direct, indirect and collider DM search experiments.

Primordial black hole (PBH) is an alternative DM candidate which does not require any new physics beyond the SM. PBHs are believed to have formed after the inflation, and subsequently evolved through accretion, mergers, and Hawking radiation. Depending on the time of formation, the masses of PBHs can vary in a large range. In general, the initial mass  $M_{\text{PBH}}$  of a PBH should be close to the Hubble horizon mass at the production time  $t$ ,  $M_{\text{PBH}} \sim c^3 t / G \simeq 10^{15} (t / 10^{-23} \text{ s}) \text{ g}$ , where  $c$  is the speed of light and  $G$  is the Newton constant. For two typical formation time  $t$  of the Planck time  $t \sim 10^{-43} \text{ s}$  and the time just before the big-bang nucleosynthesis (BBN)  $t \sim 1 \text{ s}$ , the initial PBH mass are around  $10^{-5} \text{ g}$  and  $10^5 M_{\odot}$ , respectively.

PBH can be whole or a fraction of DM. The energy fraction of PBHs relative to that of whole DM is defined as  $f_{\text{PBH}} \equiv \Omega_{\text{PBH}} / \Omega_{\text{DM}}$ , where  $\Omega_{\text{DM}}$  and  $\Omega_{\text{PBH}}$  are the energy density parameters of DM and PBHs relative to the critical density of the present Universe, respectively. For heavy PBHs with  $M_{\text{PBH}} \gg 10^{17} \text{ g}$ , the value of  $f_{\text{PBH}}$  can be constrained by the gravitational effects from PBHs such as microlensing [1–7], dynamical constraint from globular clusters, galaxy disruption and other observables [8–11] (for recent reviews, see e.g. [12, 13]).

Light PBHs are expected to emit SM particles through Hawking radiations [14]. PBHs in the mass range from  $10^{13} - 10^{17} \text{ g}$  are expected to emit SM particles with typical energies from a few GeV down to a few hundreds of keV. PBHs loss their masses through Hawking radiation at a rate  $dM_{\text{PBH}}/dt \propto M_{\text{PBH}}^{-2}$  [15, 16], which suggests that heavier PBHs evaporate slower. It has been shown that PBHs with masses  $M_{\text{PBH}} \gtrsim 5 \times 10^{14} \text{ g}$  have lifetimes larger the age of the Universe, and can be considered as stable sources of photons and cosmic-ray (CR) particles in the Galaxy [17]. This type of evaporating PBHs can be searched by current space-borne detectors. For PBHs in this mass region, the value of  $f_{\text{PBH}}$  can be constrained by the data of extragalactic and galactic diffuse  $\gamma$ -rays [18–20], CMB [21], neutrinos [22, 23], CR electrons [24], CR positron annihilation into 511 keV gamma-ray lines [22, 25], and CR antiprotons [26, 27], etc.

Recently, low-energy CR all-electron ( $e^+ + e^-$ ) flux data from Voyager-1 have been used to set constraints on  $f_{\text{PBH}}$  [24]. The obtained limits turned out to be competitive with that derived from extragalactic  $\gamma$ -rays. As Voyager-1 is now outside the heliopause, the electron

flux measured by Voyager-1 can be considered as the true local interstellar (LIS) flux, and the derived constraints are expected to be relatively robust against the influence of the solar activity, the so called solar modulation effect. Note, however, that although the low-energy electron data from Voyager-1 can be considered as the true LIS flux, the theoretical prediction for CR flux from PBH evaporation involves a number of parameters for the CR propagation in the Galaxy, such as the diffusion coefficient, re-acceleration coefficient and convection velocity. These parameters are determined through fitting to the CR data (e.g. the Boron to Carbon flux ratio, B/C) measured at the top of the atmosphere (TOA) deep inside the heliosphere, which are strongly affected by the solar activity. Thus, the constraints on the PBH fraction from the Voyager data are *inevitably* affected the solar modulation effect. Actually, the LIS fluxes measured by Voyager-1,2 are more useful in improving the modeling and calibrating of the solar modulation effect itself. In order to derive robust constraints on exotic contributions, it is necessary to consider both the LIS and TOA CR flux data simultaneously and consistently calculate the CR propagation in the Galaxy and heliosphere, as the parameters of the two processes are strongly correlated.

In this work we explore the possibility of using CR positron flux to constrain the abundance of PBHs. CR positrons are believed to be of secondary origin and relatively rare compared with the CR primaries such as protons and electrons. Thus CR positron flux should be sensitive to any exotic contributions. The currently measured CR positron flux already showed an unexpected rise starting at high energies above 20 GeV and a peak at around 300 GeV, which may hint at nearby astrophysical sources or halo DM contributions (see e.g. [28–33]). Alternatively, the low-energy CR positron flux below  $\sim 10$  GeV can be used to set constraints on exotic contributions as they are roughly consistent with the expected backgrounds. In this work, we shall use the low-energy CR positron data with kinetic energy from 0.5–5.2 GeV from AMS-02 to constrain the PBH fraction  $f_{\text{PBH}}$ . Although the initial energy of the CR positrons from evaporating PBHs with mass above  $5 \times 10^{14}$  g should be quite low around  $\mathcal{O}(10)$  MeV, the positron energy can be further enhanced during the propagation process through interacting with the galactic magnetic fields, which is known as the re-acceleration process. The existence of re-acceleration is favored by a large number of independent analyses (see, e.g. [33–42]). We use the state-of-the-art models for CR propagation in the Galaxy (based on the numerical code `Galprop` [34–38]) and in the heliosphere (using the code `Helmod` [43–47] which is based on the numerical solution of the Parker equation and the force-field approximation). In calculating the CR positron flux from PBH evaporation the numerical code `BlackHawk` [48] is used which includes both the primary and secondary contributions. The results show that for typical diffusive re-acceleration models with best-fit parameters determined from current proton, B/C and light CR nuclei data, the CR positron flux measured by AMS-02 can provide very stringent limits, which can be stronger than the previous constraints derived from the Voyager electron flux by around an order of magnitude.

The remaining part of this paper is organized as follows. In section II, we give a brief

overview on the particle spectrum from PBH evaporation. In section III, we discuss the CR propagation in the Galaxy and the models for solar modulation. The constraints on PBH abundances from the AMS-02 positron data are discussed in section IV for the cases without background and with backgrounds. The results of this work is summarized in section V.

## II. EVAPORATION OF PRIMORDIAL BLACK HOLES

In this work, unless otherwise stated, we adopt the natural system of units with  $\hbar = k_B = c = 1$ , where  $\hbar$  is the reduced Plank constant,  $k_B$  is the Boltzmann constant, and  $c$  is the speed of light. We consider a simple scenario where the spin of PBHs can be negligible, which can be obtained from a series of possible formation mechanisms [49–51] (for the formation of PBHs with near-extremal spin, see e.g. [52–54]). The emission rate of particle species  $i$  per unit time  $t$  and total energy  $E$  from Hawking radiation is given by [55]

$$\frac{d^2 N_i}{dt dE} = \frac{g_i \Gamma_i}{2\pi} \left[ \exp\left(\frac{E}{T_{\text{PBH}}}\right) - (-1)^{2s_i} \right]^{-1}, \quad (1)$$

where  $s_i$  and  $g_i$  are the spin and the total degree of freedom of the particle  $i$ , respectively, and the temperature  $T_{\text{PBH}}$  of a PBH with mass  $M_{\text{PBH}}$  is [56]

$$T_{\text{PBH}} \approx 10.6 \times \left( \frac{10^{15} \text{ g}}{M_{\text{PBH}}} \right) \text{ MeV}. \quad (2)$$

The graybody factor  $\Gamma_i$  in Eq. (1) is determined by the equation of motion of the particle in curved space time near the horizon. It describes the probability that the particle  $i$ , created at the PBH horizon, finally escapes to spatial infinity. In the geometric optics limit (i.e., the high-energy limit), the graybody factor for electron can be approximated as  $\Gamma_e \simeq 27 G^2 M_{\text{PBH}}^2 E^2$ . Note that Eq. (1) only describes the primary particles directly emitted from PBHs. The decays of the unstable primary particles can produce secondary stable particles. In the calculation of the graybody factor and the energy spectra of the emitted particles, we use the numerical code of `BlackHawk` [48, 57] in which both the primary and secondary production processes are calculated. For the low-energy particle production and decay, we use the results from the `Hazma` code [58] which is now included in the updated version `BlackHawk-v2.1` [48].

The energy spectrum  $d^2 n_{e^\pm} / dt dE_{\text{kin}}$  from all the evaporating PBHs with different masses is given by

$$\frac{d^2 n_{e^\pm}}{dt dE_{\text{kin}}} = \int_{M_{\text{min}}}^{\infty} dM_{\text{PBH}} \frac{d^2 N_{e^\pm}}{dt dE_{\text{kin}}} \frac{dn}{dM_{\text{PBH}}}, \quad (3)$$

where  $dn/dM_{\text{PBH}}$  is the mass distribution function of PBH. Depending on formation mechanisms, the mass function can be a peak theory distribution [59, 60], log-normal distribution [61], monochromatic distribution [62] or power-law distribution [63]. In this work, we consider two widely used models, namely, monochromatic and log-normal mass functions. A

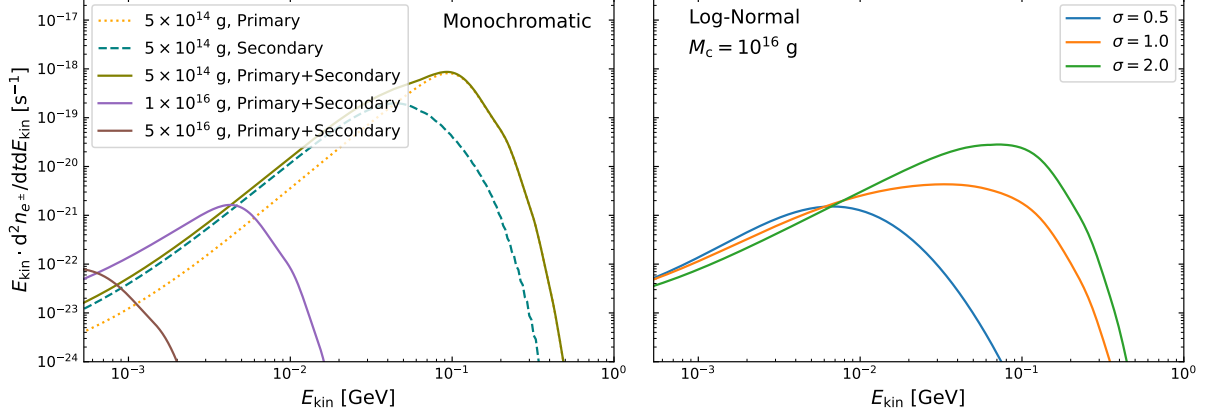


Figure 1. Left) Initial fluxes of CR positron evaporated from PBHs with monochromatic mass distribution with  $M_c = 5 \times 10^{14}$  g,  $1 \times 10^{16}$  g, and  $5 \times 10^{16}$  g. For the case of light PBHs with  $M_c = 5 \times 10^{14}$  g, the contribution from the secondary positrons are also shown as they are non-negligible. Right) The same as the left but for log-normal mass distribution with  $M_c = 5 \times 10^{16}$  g and three different widths  $\sigma = 0.5, 1.0$  and  $2.0$ .

nearly monochromatic mass function is naturally expected if all PBHs are formed at a same epoch, and a log-normal mass function can arise from inflationary fluctuations [64, 65]. The two mass functions are given by

$$\frac{dn}{dM_{\text{PBH}}} = \begin{cases} A_1 \delta(M_{\text{PBH}} - M_c) & \text{(monochromatic)} \\ \frac{A_2}{\sqrt{2\pi}\sigma M_{\text{PBH}}^2} \exp\left[-\frac{\ln^2(M_{\text{PBH}}/M_c)}{2\sigma^2}\right] & \text{(log-normal),} \end{cases} \quad (4)$$

where  $M_c$  is the characteristic mass,  $\sigma$  is the width of the log-normal mass distribution,  $A_1$  and  $A_2$  are normalized factors with different unit, which are determined by  $\rho_{\text{PBH}}$  the energy density of PBH as follows

$$\int_{M_{\text{min}}}^{\infty} M_{\text{PBH}} \frac{dn}{dM_{\text{PBH}}} dM_{\text{PBH}} = \rho_{\text{PBH}}. \quad (5)$$

Due to Hawking radiation, PBHs continually lose their masses. Analytical and numerical calculations both confirmed that the lighter PBHs, the faster evaporation [66, 67], suggesting PBHs with very small masses ( $\lesssim 5 \times 10^{14}$  g) are absent by now. In this work we only take into account the contribution from the existing PBHs, the lower bound  $M_{\text{min}}$  in Eq. (5) is fixed at  $M_{\text{min}} = 5 \times 10^{14}$  g. From Eq. (5), the relation between the normalized factor and  $\rho_{\text{PBH}}$  can be obtained. It is evident that  $A_1 = \rho_{\text{PBH}}/M_c$  for  $M_c > M_{\text{min}}$ . The value of  $A_2$  can be expressed as  $A_2 = \rho_{\text{PBH}}/k$ , where  $0.5 \lesssim k \lesssim 1$  from numerical calculations. The case of  $k = 1$  corresponds to the limit of  $M_{\text{min}} = 0$ .

In the left panel of Fig. 1, we show the calculated emission spectrum  $d^2 N_{e^\pm}/dt dE_{\text{kin}}$  for CR  $e^\pm$  as a function of kinetic energy  $E_{\text{kin}} = E - m_e$  in the monochromatically distributed

PBHs with typical masses  $M_{\text{PBH}} = 5 \times 10^{14}$  g,  $1 \times 10^{16}$  g and  $5 \times 10^{16}$  g, respectively. For light PBHs with  $M_{\text{PBH}} = 5 \times 10^{14}$  g, the contributions from secondary particles are important, the secondaries can be dominant in the low-energy region below 10 MeV and can change the spectral shape significantly. For heavier PBHs with  $M_{\text{PBH}} \gtrsim 1 \times 10^{16}$  g, the secondary contribution is negligible, so only the total contribution is shown. In the right panel of Fig. 1, the energy spectra for the case of log-normal PBH mass distribution is shown for fixed  $M_c = 1 \times 10^{16}$  g with three different widths of  $\sigma = 0.5, 1.0$  and  $2.0$ . Compared with the left panel, for larger width such as  $\sigma = 2.0$ , the spectra can extend to much higher energies, as the possibility for having lighter PBHs is significantly increase.

### III. CR PROPAGATION IN THE GALAXY AND THE HELIOSPHERE

#### A. CR propagation in the Galaxy

The propagation of CR charged particles in the Galaxy can be described by a 2D diffusion model in which a diffusion zone is assumed to be a cylinder with radius  $R_h \approx 20$  kpc and half-height  $z_h = 1 \sim 10$  kpc. The diffusion equation of CR charged particles can be written as [68, 69]:

$$\begin{aligned} \frac{\partial \psi}{\partial t} = & q(\mathbf{r}, p) + \nabla \cdot (D_{xx} \nabla \psi - \mathbf{V}_c \psi) + \frac{\partial}{\partial p} p^2 D_{pp} \frac{\partial \psi}{\partial p} \\ & - \frac{\partial}{\partial p} \left[ \dot{p} \psi - \frac{p}{3} (\nabla \cdot \mathbf{V}_c) \psi \right] - \frac{\psi}{\tau_f} - \frac{\psi}{\tau_r}, \end{aligned} \quad (6)$$

where  $\psi(\mathbf{r}, p, t)$  is the number density per unit of particle momentum  $p$  at the position  $\mathbf{r}$  which is related to the phase space distribution function  $f(\mathbf{r}, \mathbf{p}, t)$  as  $\psi(\mathbf{r}, p, t) = 4\pi p^2 f(\mathbf{r}, \mathbf{p}, t)$ ,  $q(\mathbf{r}, p)$  is the time-independent source term,  $D_{xx}$  is the energy-dependent spatial diffusion coefficient,  $\mathbf{V}_c$  is the convection velocity related to the galactic wind,  $D_{pp}$  is the diffusion coefficient in momentum space,  $\dot{p} \equiv dp/dt$  is the momentum loss rate,  $\tau_f$  and  $\tau_r$  are the time scales of particle fragmentation and radioactive decay, respectively.

The diffusion coefficient is parameterized as  $D_{xx} = \beta^\eta D_0 (\rho/\rho_0)^\delta$ , where  $\rho = p/(Ze)$  is the rigidity of the cosmic-ray particle with electric charge  $Ze$ ,  $\delta$  is the spectral power index,  $D_0$  is a constant normalization coefficient determined at rigidity 4.5 GV,  $\beta = v/c$  is the velocity of CR particles relative to the speed of light  $c$ , and the  $\eta$  parameter is introduced to accommodate the low-rigidity behavior of the CR spectra. If necessary, an ad-hoc break in  $\delta$  can be introduced, namely,  $\delta = \delta_0$  ( $\delta_1$ ) for  $\delta$  below (above) a reference rigidity  $\rho_0$ . The diffusion in momentum space is described by the parameter  $D_{pp}$  which can be parameterized as

$$D_{pp} = \frac{4V_a^2 p^2}{3D_{xx} \delta (4 - \delta^2) (4 - \delta)}, \quad (7)$$

where  $V_a$  is the Alfvén velocity which characterizes the propagation of disturbances in Galactic magnetic fields. The scattering of charged particles by the random motion of the magnetic fields characterized by the Alfvén velocity leads to a certain amount of second-order Fermi acceleration during propagation, which can significantly modify the low-energy CR energy spectrum.

The convection velocity  $\mathbf{V}_c$  is modeled as a vector field perpendicular to the galactic disk, starting from  $V_{c0}$  at  $z = 0$  and increases linearly with  $|z|$  with gradient  $dV_c/dz$ . For stable CR sources, the steady-state solution can be achieved, the corresponding condition is  $\partial\psi/\partial t = 0$ . For the boundary conditions, it is assumed that particles can escape freely at the boundary of the halo. In terms of the cylinder coordinates  $(R, z)$ , the boundary condition is  $\psi(R = R_h, z, p) = \psi(R, z = \pm z_h, p) = 0$ . The diffusion equation can be numerically solved use the public code `GALPROP` [34–38].

The primary CR electrons are believed to be accelerated by supernova remnants (SNR) and pulsar wind nebulae. The distribution of the primary CR sources can be modeled by a spatial density function multiplied by a broken power-law spectrum with  $m$ -fold breaks at rigidities  $\rho_i$ , ( $i = 1, \dots, m$ ) with indices  $\gamma_i$  before each break

$$q(\mathbf{r}, p) = n(\mathbf{r}) \left(\frac{\rho}{\rho_0}\right)^{-\gamma_0} \prod_{i=0}^{m-1} \left[\frac{\max(\rho, \rho_i)}{\rho_i}\right]^{-\gamma_{i+1}}. \quad (8)$$

For instance, if only one break at  $\rho_0$  is considered, the source power term has two power indices  $\gamma_0$  and  $\gamma_1$ . The spatial distribution of the primary sources is assumed to follow that of SNRs, which is parameterized as follows

$$n(R, z) \propto \left(\frac{R}{r_\odot}\right)^a \exp\left(-b\frac{R - r_\odot}{r_\odot}\right) \exp\left(-\frac{|z|}{0.2 \text{ kpc}}\right), \quad (9)$$

where the two source parameters  $a$  and  $b$  slightly depends on CR species.

In addition to the primary CR electrons, there are secondary CR  $e^\pm$  created by the collision of primary CR nuclei with the interstellar medium (ISM). The secondary source term for CR electrons and positrons is given by

$$q_{e^\pm}^{\text{sec}}(\mathbf{r}, p) = \sum_{ij} n_j(\mathbf{r}) \int dp'_i c\beta_i \psi_i(\mathbf{r}, p'_i) \frac{d\sigma^{ij \rightarrow e^\pm}(p, p'_i)}{dp}, \quad (10)$$

where the index  $i$  runs through primary CR particles such as proton and Helium,  $\beta_i$  is the velocity of primary CR particle  $i$ ,  $n_j$  is the number density of the  $j$ -th ISM component with  $j$  runs through HI, HII, and H<sub>2</sub>,  $d\sigma^{ij \rightarrow e^\pm}(p, p'_i)/dp$  is the differential cross-section for creating a secondary  $e^\pm$  with momentum  $p$  from an incident primary particle  $i$  with momentum  $p'_i$ . Secondary  $e^\pm$  are typically produced from the decay of  $\pi^\pm$  and  $K^\pm$  during the collision with ISM [70].

## B. CR propagation in the Heliosphere

In the vicinity of the Sun, the propagation of charged CR particles is affected by the regular and irregular heliospheric magnetic fields generated by the out flowing solar wind. The solar activity leads to time-dependent suppression of the CR particle flux with rigidity below  $\sim 50$  GV, which is referred to as the solar modulation effect. The CR propagation in the heliosphere can be described by the following Parker equation

$$\frac{\partial U}{\partial t} = \nabla \cdot (K^S \nabla U - (\mathbf{V}_{\text{sw}} + v_d)U) + \frac{1}{3} \nabla \cdot \mathbf{V}_{\text{sw}} \frac{\partial}{\partial T} (\alpha_{\text{rel}} E_{\text{kin}} U), \quad (11)$$

where  $U(\mathbf{r}, t, E_{\text{kin}})$  is the particle number density per kinetic energy  $E_{\text{kin}}$ ,  $K^S$  is the symmetric part of the diffusion tensor,  $V_{\text{sw}}$  is the solar wind velocity,  $v_d$  is the particle magnetic drift velocity, and  $\alpha_{\text{rel}} = (E_{\text{kin}} + 2m)/(E_{\text{kin}} + m)$ . The component of  $K^S$  parallel to the magnetic field  $K_{\parallel}$  is believed to be dominant over that perpendicular component  $K_{\perp}$ . The parallel component is parametrized as

$$K_{\parallel} = \frac{\beta}{3} K_0 \left( \frac{\rho}{1 \text{ GV} + g_{\text{low}}} \right) \left( 1 + \frac{r}{1 \text{ AU}} \right), \quad (12)$$

where  $K_0$  is the diffusion parameter and  $r$  is the distance to the Sun,  $g_{\text{low}}$  is a parameter depends on the solar activity. The  $i$ -th perpendicular component  $K_{\perp,i}$  is related to the parallel component through  $K_{\perp,i} = \rho_i K_{\parallel}$ . The parameters  $g_{\text{low}}$  and  $\rho_i$  are two major free parameters which need to be determined by the CR data measured at different period of solar activities. The Parker equation can be numerically solved with the results summarized in the code `Helmod` [43–47] in which the propagation parameters are calibrated using the up-to-date CR data. The `Helmod` code is able to quantitatively reproduce the time variation of CR fluxes such as that of protons, and the predicted LIS proton flux is in a remarkable agreement with the Voyager-1 data [46].

Another commonly-adopted model for solar modulation is based on the simplified force-field approximation [71]. In this approach, the CR flux  $\Phi$  at TOA is related to that at LIS through the relation

$$\Phi^{\text{TOA}}(E_{\text{kin}}^{\text{TOA}}) = \left( \frac{2mE_{\text{kin}}^{\text{TOA}} + (E_{\text{kin}}^{\text{TOA}})^2}{2mE_{\text{kin}} + E_{\text{kin}}^2} \right) \Phi(E_{\text{kin}}). \quad (13)$$

The kinetic energy  $E_{\text{kin}}$  of the CR particle in LIS is related to that at TOA through the relation  $E_{\text{kin}} = E_{\text{kin}}^{\text{TOA}} + e\phi_F|Z|$ , where  $\phi_F$  is the so-called Fisk potential which is a phenomenological parameter needs be determined together with other propagation parameters. In this method, the solar modulation effect is assumed to be homogeneous. The value of  $\phi_F$  is dependent on the CR species, and different values of  $\phi_F$  should be adopted to fit the same CR specie measured at different time period. There is a strong degeneracy between  $\phi_F$  and the CR propagation parameters and the primary source parameters.



### C. Benchmark propagation models

In this work, we take the analysis framework of `Galprop+Helmod` as the benchmark model. In this framework, the two numerical codes `Galprop` and `Helmod` are combined together to provide a single framework to calculate CR fluxes at different modulation levels and at both polarities of the solar magnetic field [40, 41, 72, 73]. This is achieved by an iterative optimization procedure to tune the parameters in both `Galprop` and `Helmod` to best reproduce the data set of CR proton flux measured by PAMELA, BESS and AMS-02. The prediction LIS proton spectrum is in a remarkable agreement with the Voyager-1 data [46]. We adopt the best parameters determined in [41] which is obtained by a MCMC scan of the parameter space to fit the AMS-02 data of light nuclei. In this model (referred to as model-GH), the best fit halo height is fixed at  $z_h = 4$  kpc. The details of the parameters of these propagation models are listed in the first column of Table I. In this model, the source parameters in Eq. (9) are fixed at  $a = 1.9$  and  $b = 5.0$ .

Parameters	GH	MIN	MED	MAX
$z_h$ [kpc]	4.0	1.8	3.2	6.0
$D_0$ [ $10^{28}$ cm <sup>2</sup> s <sup>-1</sup> ]	4.3	3.5	6.5	10.6
$\eta$	0.7	1	1	1
$\delta$	0.415	0.30	0.29	0.29
$V_a$ [km s <sup>-1</sup> ]	30	42.7	44.8	43.4
$dV_c/dz$ [km s <sup>-1</sup> kpc <sup>-1</sup> ]	9.8	–	–	–
$\phi_F$ [GV]	–	0.55	0.55	0.55
$\rho_0$ [GV]	0.95	4.0	4.0	4.0
$\gamma_0$	2.24	1.75	1.79	1.81
$\gamma_1$	1.70	2.44	2.45	2.46

Table I. Best-fit parameters for the four CR propagation models GH [41], MIN, MED and MAX [33]. The primary index  $\gamma_{0,1}$  and break rigidity  $\rho_0$  are for CR primary protons.

For the framework with `Galprop`+ $\phi_F$ , we consider the best-fit parameters from our previous analysis to the AMS-02 proton and B/C data [33]. Three representative models with different values of  $z_h = 2-6$  kpc (the so called MIN, MED and MAX models for `Galprop`) are considered to take into account the large uncertainties in  $z_h$  due to the well-known  $z_h - D_0$  degeneracy. The solar potential for these three models are fixed at  $\phi_F = 550$  MV. The details of the parameters of these propagation models are listed in Table I. In this model, slightly different values of the source parameters  $a = 1.25$  and  $b = 3.56$  are adopted, which are also the default values used by `Galprop-v54`.

In the calculation of primary CR sources from PBH evaporation, the spatial distribution of PBHs in the Galaxy is assumed to follow that of DM, namely,  $\rho_{\text{PBH}}(r)$  satisfies  $\rho_{\text{PBH}}(r) =$

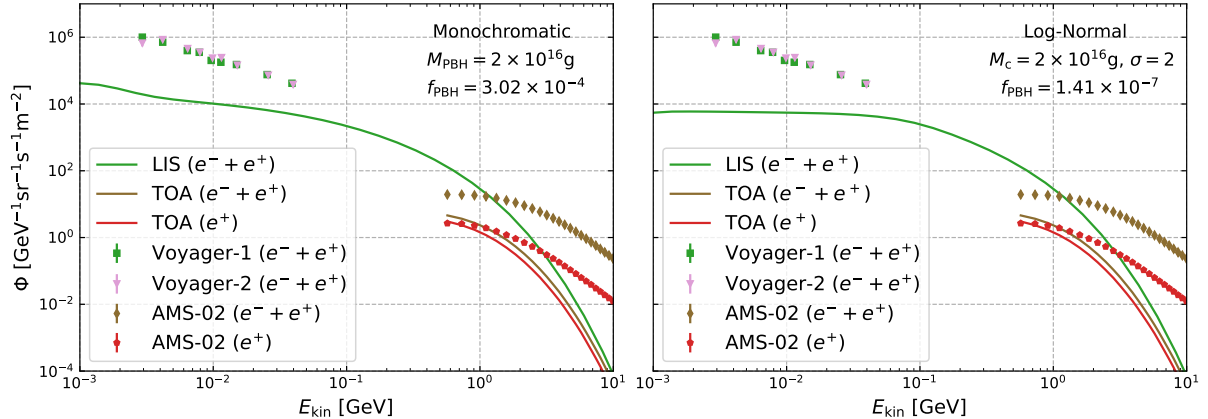


Figure 2. Left) LIS and TOA CR positron and all-electron fluxes from the evaporation of PBHs in the GH propagation model. The PBH mass distribution is taken to be monochromatic with  $M_c = 2 \times 10^{16}$  g. The data of Voyager-1,2 (all-electron) [75] and AMS-02 (positron and all-electron) [76] are also shown. The value of  $f_{\text{PBH}}$  is chosen to saturate the AMS-02 positron data at lowest kinetic energy at 0.5 GeV. Right) The same as the left but for PBH log-normal mass distribution with  $M_c = 2 \times 10^{16}$  g and  $\sigma = 2.0$ .

$f_{\text{PBH}} \cdot \rho_{\text{DM}}(r)$ , where  $\rho_{\text{DM}}(r)$  is the DM density profile. We consider the Navarro-Frenk-White (NFW) profile [74]

$$\rho_{\text{DM}}(r) = \rho_0 \left(1 + \frac{r_{\odot}}{r_s}\right)^2 \left(\frac{r}{r_{\odot}}\right)^{-1} \left(1 + \frac{r}{r_s}\right)^{-2}, \quad (14)$$

where  $\rho_0 = 0.43 \text{ GeV} \cdot \text{cm}^{-3}$  is the local DM energy density,  $r_{\odot} = 8.5 \text{ kpc}$  is the distance of the Sun to the Galactic center, and  $r_s = 20 \text{ kpc}$  is a typical radius parameter. Note that for CR electron and positron fluxes the DM profile dependence is rather weak.

In the left panel of Fig. 2, we show the CR positron and all-electron ( $e^- + e^+$ ) flux predicted from the evaporation of PBHs with monochromatic mass  $M_{\text{PBH}} = 2 \times 10^{16}$  g in the GH propagation model together with the data of AMS-02 (positron and all-electron) and Voyager-1, -2 (all-electron). The astrophysical background electrons and positrons are not shown for the moment, such that conservative constraints (i.e. the constraints without including the astrophysical backgrounds) on  $f_{\text{PBH}}$  can be roughly estimated from comparing the theoretical predictions with the data. It can be seen that in the propagation model under consideration, the PBH generated positron flux will be first constrained by the AMS-02 positron data in the GeV region rather than that from the Voyager all-electron data in the MeV region. Since the predicted CR fluxes depend on  $f_{\text{PBH}}$  linearly, we find by gradually increasing the value of  $f_{\text{PBH}}$  that for  $f_{\text{PBH}} \approx 3 \times 10^{-4}$  the predicted positron flux can saturate the low-energy positron flux at  $\sim 0.5$  GeV measured by AMS-02, which will set the scale of the final constraints from a statistic analysis. We find similar results for other propagation models such as the MIN, MED and MAX models. In the right panel of Fig. 2, we show

the result for the log-normal mass function with  $M_c = 2 \times 10^{16}$  g and width  $\sigma = 2$  in the propagation model GH. The CR backgrounds are also neglected in the panel in order to estimate the conservative constraints on  $f_{\text{PBH}}$ . It can be seen that in this extended mass function the value of  $f_{\text{PBH}}$  will again be constrained first by the AMS-02 low-energy positron data. A typical value is  $f_{\text{PBH}} \lesssim 1.4 \times 10^{-7}$ .

For PBHs with  $M_{\text{PBH}} \sim \mathcal{O}(10^{16})$  g, the corresponding PBH temperatures are only around  $\mathcal{O}(\text{MeV})$ . Thus the positrons evaporated from the PBH should have very low MeV-scale initial energies. The fact that a significant portion of the CR positrons can reach the GeV region after the propagation is closely related to the re-acceleration term in the CR propagation model in Eq. (7) with a sizable value of  $V_a$ . During the CR propagation process, it is generally expected that charged CR particles can be accelerated by the random motion of the Galactic magnetic fields, and it is well-known that it provides a natural mechanism to reproduce the low-energy B/C ratio with Kolmogorov type turbulence [77]. Diffusive re-acceleration is now a standard term in the `Galprop` code [34–38] and also in the `Dragon` code [42] for CR propagation. In the `Galprop+Helmod` analysis framework, the recently fit including AMS-02 data of Li, Be and B fluxes strongly favor  $V_a \sim 30$  km/s [40, 41]. In the `Galprop+ $\phi_F$`  framework, a recent analysis including the AMS-02 data of Be–O nuclei also favored a large  $V_a \sim 30$  km/s, although it was also noticed that fit to another data set of proton, antiproton, and Helium tended to give a smaller value of  $V_a$  [39]. An alternative explanation to the observed structure of the B/C data is to introduce *ad-hoc* breaks in the diffusion coefficient. A recent analysis showed that the two competing scenarios, one with re-acceleration and the other one without re-acceleration but with a break in the diffusion can fit the AMS data of Li – O nuclei well, after the uncertainties in the cross sections are taken into account [78]. Similar conclusions can be found in fitting only to the AMS-02 B/C data using the semi-analytic 1D propagation models [79]. At present, although the re-acceleration process is generally expected, the exact value of  $V_a$  is not yet conclusive. Fig. 2 suggest that if a large  $V_a$  of  $\sim 30$  km  $\cdot$  s $^{-1}$  is confirmed, the AMS-02 positron data will be more powerful in constraining  $f_{\text{PBH}}$  than that from the Voyager all-electron data.

#### IV. CONSTRAINTS ON THE PBH ABUNDANCE

In this section, we derive the constraints on  $f_{\text{PBH}}$  from the current CR electron and positron data. In the first step, we derive the constraints under the assumption of null astrophysical backgrounds, which should be more conservative and robust compared with that with astrophysical backgrounds included. In calculating the constraints, we adopt a simple approach by requiring that the predicted CR flux from PBH evaporation should not exceed the measured value by more than  $2 \sigma$  uncertainty in any energy bin, which was adopted in Ref. [24], and allows for a direct comparison with their results. The constraints can be obtained by simply rescaling the value of  $f_{\text{PBH}}$  and compare the predictions with the

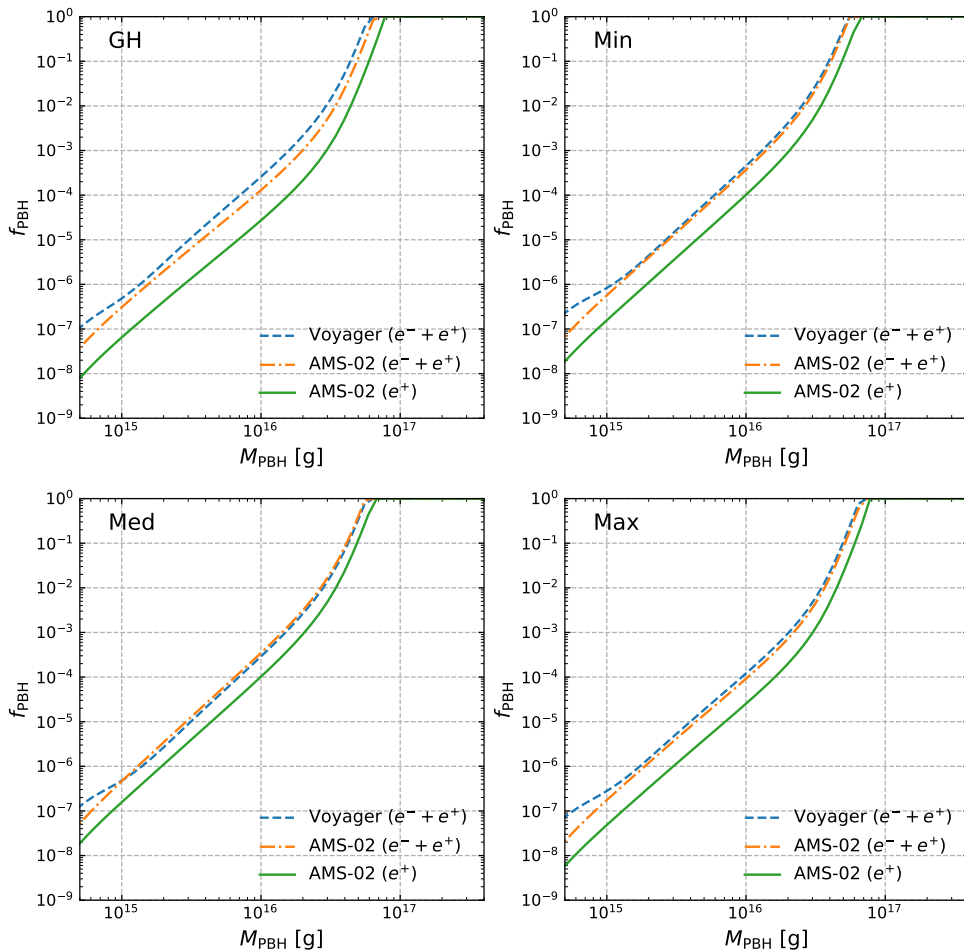


Figure 3. Constraints on  $f_{\text{PBH}}$  in four CR propagation models GH [41], MIN, MED, MAX [33] with parameters listed in Tab. I. The blue, orange, and green curves represent the constraints obtained individually from the all-electron data of Voyager-1,2 [75], the all-electron data of AMS-02 [76], and the positron data of AMS-02 [76], respectively. The monochromatic PBH mass function is assumed in all the panels.

experimental data.

In Fig. 3, we show the obtained individual constraints from Voyager-1,2 all-electron data, AMS-02 all-electron data and AMS-02 positron data for monochromatically distributed PBHs in the mass range  $5 \times 10^{14} - 10^{17}$  g. The results for four different propagation models GH, MIN, MED and MAX listed in Tab. I are shown in the four panels of Fig. 3. It can be seen from the figure that for all the four propagation models, the constraints from the low-energy AMS-02 positron data are the most stringent. In the GH propagation model, we obtain conservative upper limit of

$$f_{\text{PBH}} \lesssim 3 \times 10^{-4} \text{ at } M_{\text{PBH}} \simeq 2 \times 10^{16} \text{ g},$$

which is stronger than that from the Voyager all-electron data by an order of magnitude. The

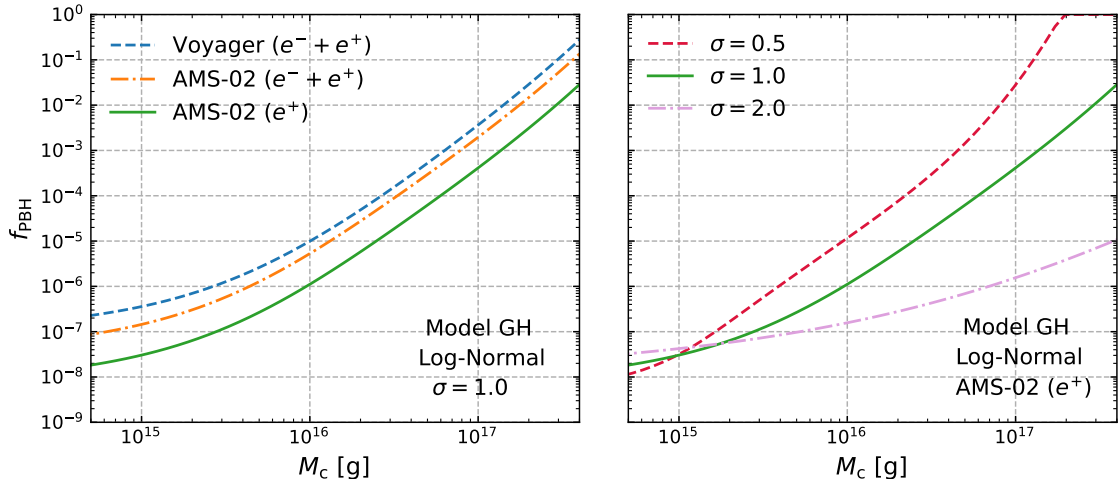


Figure 4. Left) Constraints on  $f_{\text{PBH}}$  in the GH propagation model with parameters listed in Tab. I. The blue, orange, and green curves represent the constraints obtained individually from the all-electron data of Voyager-1,2 [75], the all-electron data of AMS-02 [76], and the positron data of AMS-02 [76], respectively. The log-normal PBH mass function with width  $\sigma = 1.0$  is assumed. Right) The constraints from the AMS-02 positron data only, for the log-normal PBH mass function with different widths of  $\sigma = 0.5, 1.0$  and  $2.0$ , respectively.

AMS-02 positron constraints are also more stringent than that from the AMS-02 all-electron data. The reason is that the initial spectra of electrons and positrons from PBH evaporation are the same as the evaporation process is charge symmetric. Thus the prediction for all-electron flux from PBH evaporation should be approximately twice the positron flux. However, the all-electron flux measured by AMS-02 is around an order of magnitude higher than of positron flux. Thus the corresponding constraints are significantly weaker in the null background case. The constraints derived in Fig. 3 are in a good agreement with the values previously estimated from the left panel of Fig. 2. In the left panel of Fig. 4 we show the constraints for log-normally distributed PBHs with a typical width  $\sigma = 1$  in the GH propagation model. Similar to the case with monochromatic mass function, the AMS-02 positron data provide the most stringent limits in the case with log-normal mass function. In the right panel of Fig. 4, the constraints for different widths  $\sigma = 0.5, 1.0$  and  $2.0$  for the log-normal mass function are compared. For the log-normal mass function constraints becomes more stringent as the value of  $\sigma$  increases, which is consistent with the flux predictions in the right panel of Fig. 2.

In the next step, we consider the CR-positron constraints including the secondary positron backgrounds. Including the astrophysical background in general results in more stringent constraints. Note, however, that so far the theoretical predictions for low-energy (sub-GeV) positron flux still suffer from significant uncertainties. In addition to the uncertainties in the propagation model such as the diffusion halo half-height  $z_h$ , large uncertainties arise from the

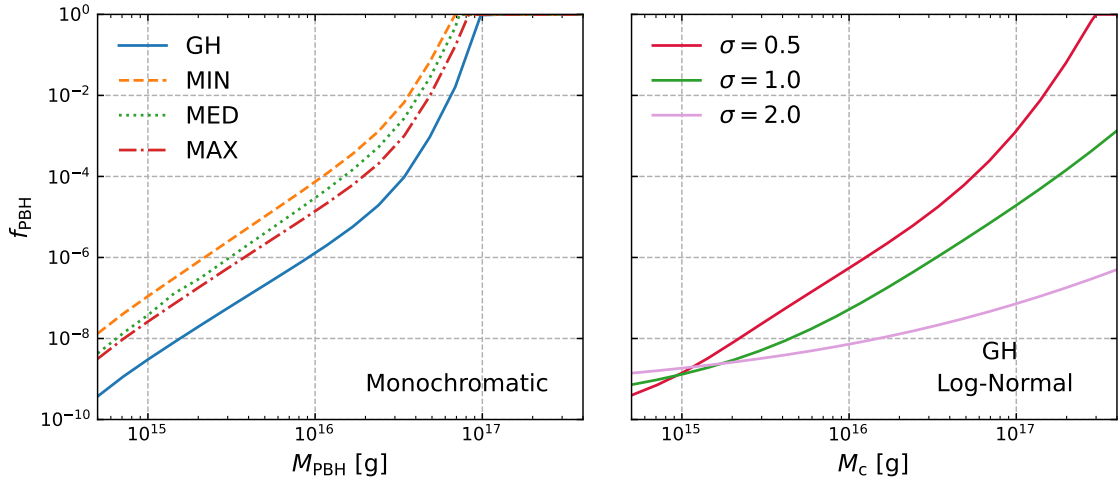


Figure 5. Left) Constraints on  $f_{\text{PBH}}$  from the AMS-02 positron data with the inclusion of astrophysical backgrounds in four CR propagation models. The PBH mass function is assumed to be monochromatic. Right) The constraints for the log-normal PBH mass function with different widths  $\sigma = 0.5, 1.0, 2.0$  in the GH propagation model.

poorly known low-energy  $pp$  and  $pA$  inelastic scattering cross sections for positron production. At present, the cross sections can be obtained either from analytical parameterizations to the experimental data [80–82] or from QCD-based Monte-Carlo event generators [83–85]. The difference can easily reach a factor of two. Other uncertainties specifically related to CR electron and positron energy loss involve that in the Galactic magnetic fields and gas distribution (for recently analyses, see e.g. [83, 86]). Thus the constraints including the astrophysical backgrounds are less robust compared with that without backgrounds. To account for the uncertainties in the secondary positron flux, we add two additional parameters  $N_{e^+}$  and  $\delta_{e^+}$  to the calculated CR positron flux  $\Phi$  from a given propagation model, namely,  $\Phi(E_{\text{kin}}) \rightarrow N_{e^+} E_{\text{kin}}^{\delta_{e^+}} \Phi(E_{\text{kin}})$ . The two parameters are determined by fitting to the experimental data. In the GH propagation model, a  $\chi^2$  fitting to the AMS-02 positron flux data in the low-energy region 0.5 – 5.2 GeV (16 data points in total) gives  $N_{e^+} = 0.255 \pm 0.003$ , and  $\delta_{e^+} = 0.995 \pm 0.010$  with  $\chi^2/\text{d.o.f} = 32.51/14$ . For other propagation models MIN, MED and MAX similar results are found.

In the presence of backgrounds, we derive the corresponding constraint on  $f_{\text{PBH}}$  using the standard minimal chi-squared method (or, the log likelihood ratio method). For a given mass function parameters of  $M_c$  or a pair of  $(M_c, \sigma)$ , we first find the best-fit parameters  $(f_{\text{PBH}}, N_{e^+}, \delta_{e^+})$  and the corresponding minimal value of  $\chi_{\text{min}}^2$ . Then, we increase the value of  $f_{\text{PBH}}$  and redo the fitting with respect to the other nuisance parameters  $N_{e^+}, \delta_{e^+}$  and obtain another value of  $\chi^2$ . This process is repeated until a particular  $f_{\text{PBH}}$  satisfying  $\Delta\chi^2 \equiv \chi^2(f_{\text{PBH}}, \hat{N}_{e^+}, \hat{\delta}_{e^+}) - \chi_{\text{min}}^2 = 3.84$  is found. Here, the parameters with a single hat minimized the  $\chi^2$  function for the given  $f_{\text{PBH}}$ . The obtained value of  $f_{\text{PBH}}$  corresponds to the

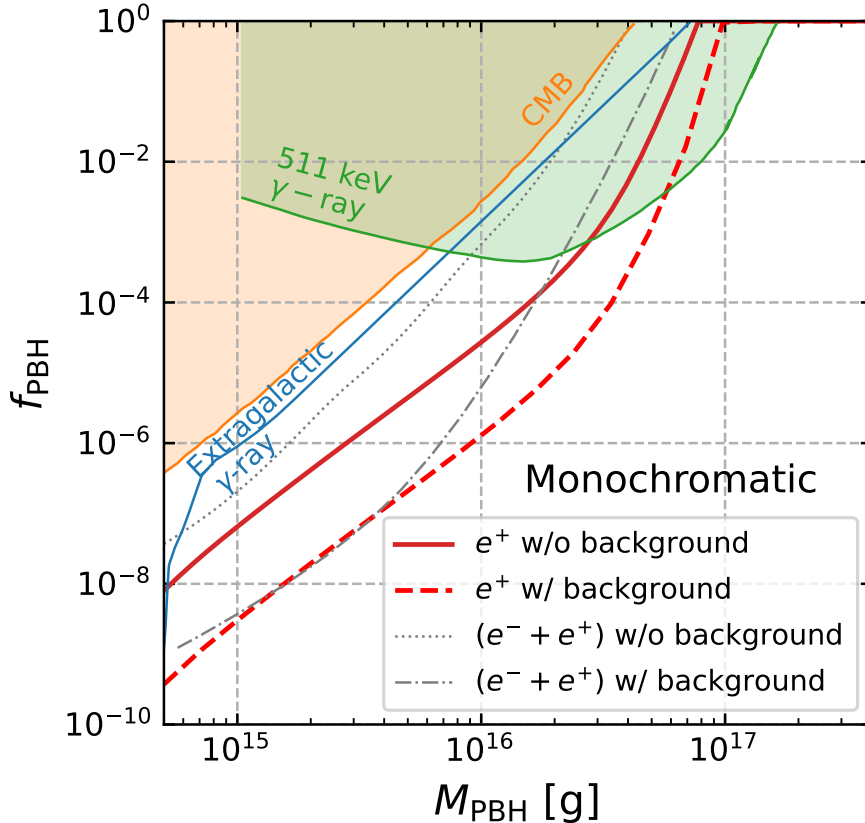


Figure 6. Exclusion lines of PBHs abundance  $f_{\text{PBH}}$ . Shadow regions are obtained from different observable, including extragalactic  $\gamma$ -rays [18], 511 keV  $\gamma$ -ray [22], CMB [21]. The dotted and dot-dashed lines are the exclusion lines originally obtained in Ref. [24]. The red-solid and red-dashed lines are the results of this work with the employments of model GH and monochromatic mass function, corresponding to the case of including and neglecting CR background, respectively.

value excluded at the 95% confidence level. In the left panel of Fig. 5, we show the obtained constraints on  $f_{\text{PBH}}$  as a function of  $M_c$  in the case of monochromatic mass function in four propagation models. The difference between different propagation models are typically within two orders of magnitude. Among these models, GH model give the most stringent limits. In the right panel of Fig. 5, the constraints for the log-normal mass function with three width  $\sigma = 0.5, 1.0, 2.0$  in the GH propagation model are shown. Similar to the right panel of Fig. 4, increasing  $\sigma$  leads to more stringent constraints. In all the case, we have verified that the constraints from the low-energy AMS-02 positron data are always the most stringent compared with that from the AMS-02 all-electron or the Voyager-1,2 all-electron data.

In Fig. 6, we compare the constraints from the AMS-02 positron data obtained in the GH model with a selection of constraints from other observables such as that from the extragalactic  $\gamma$ -ray [18], CMB [21] and 511 keV  $\gamma$ -ray line [22]. We also compare our results with

that previously obtained from the Voyager-1 all-electron data in a diffusive-reacceleration propagation model (model A) in Ref. [24]. The figure shows that the constraints from AMS-02 positron data are competitive with all these previously obtained constraints, and more stringent than that from the Voyager all-electron data in both the cases with and without including the astrophysical backgrounds.

## V. CONCLUSIONS

In summary, in this work we have explored the possibility of using the low-energy CR positron data to constrain the abundance of primordial black holes. The advantage of using the CR positron data is based on its secondary origin and thus sensitive to any exotic contributions. We have shown that in some typical diffusive re-acceleration CR propagation models, the current AMS-02 data can place stringent constraints on  $f_{\text{PBH}}$ . As an example, we have shown that in the Galprop+Helmod model for CR propagation in the Galaxy and heliosphere, a conservative upper limit of  $f_{\text{PBH}} \lesssim 3 \times 10^{-4}$  at  $M_{\text{PBH}} \simeq 2 \times 10^{16}$  g can be obtained, which improves the previous constraints from the Voyager-1 data of all-electrons by around an order of magnitude. Compared with other observables such as diffusive  $\gamma$ -rays, using the CR flux data to constrain PBH abundance in general suffers from uncertainties in the propagation models, which are expected to be improved in the near future with more precise data from the experiments such as AMS-02, DAMPE and HERD.

## ACKNOWLEDGMENTS

This work is supported in part by the NSFC under Grants No. 11825506, and No. 11821505.

- 
- [1] **MACHO** Collaboration, C. Alcock *et al.*, “The MACHO project: Microlensing results from 5.7 years of LMC observations,” *Astrophys. J.* **542** (2000) 281–307, [arXiv:astro-ph/0001272](#).
  - [2] L. Wyrzykowski *et al.*, “The OGLE View of Microlensing towards the Magellanic Clouds. III. Ruling out sub-solar MACHOs with the OGLE-III LMC data,” *Mon. Not. Roy. Astron. Soc.* **413** (2011) 493, [arXiv:1012.1154](#) [[astro-ph.GA](#)].
  - [3] L. Wyrzykowski *et al.*, “The OGLE View of Microlensing towards the Magellanic Clouds. IV. OGLE-III SMC Data and Final Conclusions on MACHOs,” *Mon. Not. Roy. Astron. Soc.* **416** (2011) 2949, [arXiv:1106.2925](#) [[astro-ph.GA](#)].
  - [4] **Macho** Collaboration, R. A. Allsman *et al.*, “MACHO project limits on black hole dark matter in the 1-30 solar mass range,” *Astrophys. J. Lett.* **550** (2001) L169, [arXiv:astro-ph/0011506](#).



- [5] K. Griest, A. M. Cieplak, and M. J. Lehner, “Experimental Limits on Primordial Black Hole Dark Matter from the First 2 yr of Kepler Data,” *Astrophys. J.* **786** no. 2, (2014) 158, [arXiv:1307.5798 \[astro-ph.CO\]](#).
- [6] S. Calchi Novati, S. Mirzoyan, P. Jetzer, and G. Scarpetta, “Microlensing towards the SMC: a new analysis of OGLE and EROS results,” *Mon. Not. Roy. Astron. Soc.* **435** (2013) 1582, [arXiv:1308.4281 \[astro-ph.GA\]](#).
- [7] K. Griest, A. M. Cieplak, and M. J. Lehner, “New Limits on Primordial Black Hole Dark Matter from an Analysis of Kepler Source Microlensing Data,” *Phys. Rev. Lett.* **111** no. 18, (2013) 181302.
- [8] S. M. Koushiappas and A. Loeb, “Dynamics of Dwarf Galaxies Disfavor Stellar-Mass Black Holes as Dark Matter,” *Phys. Rev. Lett.* **119** no. 4, (2017) 041102, [arXiv:1704.01668 \[astro-ph.GA\]](#).
- [9] M. A. Monroy-Rodríguez and C. Allen, “The end of the MACHO era- revisited: new limits on MACHO masses from halo wide binaries,” *Astrophys. J.* **790** no. 2, (2014) 159, [arXiv:1406.5169 \[astro-ph.GA\]](#).
- [10] B. Carr, “Primordial black holes as dark matter and generators of cosmic structure,” *Astrophys. Space Sci. Proc.* **56** (2019) 29–39, [arXiv:1901.07803 \[astro-ph.CO\]](#).
- [11] **MUSE** Collaboration, S. L. Zoutendijk *et al.*, “The MUSE-Faint survey: I. Spectroscopic evidence for a star cluster in Eridanus 2 and constraints on MACHOs as a constituent of dark matter,” *Astron. Astrophys.* **635** (2020) A107, [arXiv:2001.08790 \[astro-ph.GA\]](#).
- [12] B. Carr, K. Kohri, Y. Sendouda, and J. Yokoyama, “Constraints on primordial black holes,” *Rept. Prog. Phys.* **84** no. 11, (2021) 116902, [arXiv:2002.12778 \[astro-ph.CO\]](#).
- [13] B. Carr and F. Kuhnel, “Primordial Black Holes as Dark Matter: Recent Developments,” *Ann. Rev. Nucl. Part. Sci.* **70** (2020) 355–394, [arXiv:2006.02838 \[astro-ph.CO\]](#).
- [14] S. W. Hawking, “Black hole explosions,” *Nature* **248** (1974) 30–31.
- [15] I. Baldes, Q. Decant, D. C. Hooper, and L. Lopez-Honorez, “Non-Cold Dark Matter from Primordial Black Hole Evaporation,” *JCAP* **08** (2020) 045, [arXiv:2004.14773 \[astro-ph.CO\]](#).
- [16] A. Cheek, L. Heurtier, Y. F. Perez-Gonzalez, and J. Turner, “Primordial black hole evaporation and dark matter production. I. Solely Hawking radiation,” *Phys. Rev. D* **105** no. 1, (2022) 015022, [arXiv:2107.00013 \[hep-ph\]](#).
- [17] J. H. MacGibbon, “Quark and gluon jet emission from primordial black holes. 2. The Lifetime emission,” *Phys. Rev. D* **44** (1991) 376–392.
- [18] B. J. Carr, K. Kohri, Y. Sendouda, and J. Yokoyama, “New cosmological constraints on primordial black holes,” *Phys. Rev. D* **81** (2010) 104019, [arXiv:0912.5297 \[astro-ph.CO\]](#).
- [19] B. J. Carr, K. Kohri, Y. Sendouda, and J. Yokoyama, “Constraints on primordial black holes from the Galactic gamma-ray background,” *Phys. Rev. D* **94** no. 4, (2016) 044029, [arXiv:1604.05349 \[astro-ph.CO\]](#).

- [20] A. Arbey, J. Auffinger, and J. Silk, “Constraining primordial black hole masses with the isotropic gamma ray background,” *Phys. Rev. D* **101** no. 2, (2020) 023010, [arXiv:1906.04750 \[astro-ph.CO\]](#).
- [21] J. Auffinger, “Primordial black hole constraints with Hawking radiation—A review,” *Prog. Part. Nucl. Phys.* **131** (2023) 104040, [arXiv:2206.02672 \[astro-ph.CO\]](#).
- [22] B. Dasgupta, R. Laha, and A. Ray, “Neutrino and positron constraints on spinning primordial black hole dark matter,” *Phys. Rev. Lett.* **125** no. 10, (2020) 101101, [arXiv:1912.01014 \[hep-ph\]](#).
- [23] S. Wang, D.-M. Xia, X. Zhang, S. Zhou, and Z. Chang, “Constraining primordial black holes as dark matter at JUNO,” *Phys. Rev. D* **103** no. 4, (2021) 043010, [arXiv:2010.16053 \[hep-ph\]](#).
- [24] M. Boudaud and M. Cirelli, “Voyager 1  $e^\pm$  Further Constrain Primordial Black Holes as Dark Matter,” *Phys. Rev. Lett.* **122** no. 4, (2019) 041104, [arXiv:1807.03075 \[astro-ph.HE\]](#).
- [25] R. Laha, “Primordial Black Holes as a Dark Matter Candidate Are Severely Constrained by the Galactic Center 511 keV  $\gamma$ -Ray Line,” *Phys. Rev. Lett.* **123** no. 25, (2019) 251101, [arXiv:1906.09994 \[astro-ph.HE\]](#).
- [26] K. Maki, T. Mitsui, and S. Orito, “Local flux of low-energy anti-protons from evaporating primordial black holes,” *Phys. Rev. Lett.* **76** (1996) 3474–3477, [arXiv:astro-ph/9601025](#).
- [27] A. Barrau, G. Boudoul, F. Donato, D. Maurin, P. Salati, and R. Taillet, “Anti-protons from primordial black holes,” *Astron. Astrophys.* **388** (2002) 676, [arXiv:astro-ph/0112486](#).
- [28] L. Bergstrom, T. Bringmann, and J. Edsjo, “New Positron Spectral Features from Supersymmetric Dark Matter - a Way to Explain the PAMELA Data?,” *Phys. Rev. D* **78** (2008) 103520, [arXiv:0808.3725 \[astro-ph\]](#).
- [29] M. Cirelli, M. Kadastik, M. Raidal, and A. Strumia, “Model-independent implications of the  $e^\pm$ , anti-proton cosmic ray spectra on properties of Dark Matter,” *Nucl. Phys. B* **813** (2009) 1–21, [arXiv:0809.2409 \[hep-ph\]](#). [Addendum: *Nucl.Phys.B* 873, 530–533 (2013)].
- [30] L. Bergstrom, J. Edsjo, and G. Zaharijas, “Dark matter interpretation of recent electron and positron data,” *Phys. Rev. Lett.* **103** (2009) 031103, [arXiv:0905.0333 \[astro-ph.HE\]](#).
- [31] S.-J. Lin, Q. Yuan, and X.-J. Bi, “Quantitative study of the AMS-02 electron/positron spectra: Implications for pulsars and dark matter properties,” *Phys. Rev. D* **91** no. 6, (2015) 063508, [arXiv:1409.6248 \[astro-ph.HE\]](#).
- [32] H.-B. Jin, Y.-L. Wu, and Y.-F. Zhou, “Implications of the first AMS-02 measurement for dark matter annihilation and decay,” *JCAP* **11** (2013) 026, [arXiv:1304.1997 \[hep-ph\]](#).
- [33] H.-B. Jin, Y.-L. Wu, and Y.-F. Zhou, “Cosmic ray propagation and dark matter in light of the latest AMS-02 data,” *JCAP* **09** (2015) 049, [arXiv:1410.0171 \[hep-ph\]](#).
- [34] A. W. Strong and I. V. Moskalenko, “Propagation of cosmic-ray nucleons in the galaxy,” *Astrophys. J.* **509** (1998) 212–228, [arXiv:astro-ph/9807150](#).

- [35] I. V. Moskalenko, A. W. Strong, J. F. Ormes, and M. S. Potgieter, “Secondary anti-protons and propagation of cosmic rays in the galaxy and heliosphere,” *Astrophys. J.* **565** (2002) 280–296, [arXiv:astro-ph/0106567](#).
- [36] A. W. Strong and I. V. Moskalenko, “Models for galactic cosmic ray propagation,” *Adv. Space Res.* **27** (2001) 717–726, [arXiv:astro-ph/0101068](#).
- [37] I. V. Moskalenko, A. W. Strong, S. G. Mashnik, and J. F. Ormes, “Challenging cosmic ray propagation with antiprotons. Evidence for a fresh nuclei component?,” *Astrophys. J.* **586** (2003) 1050–1066, [arXiv:astro-ph/0210480](#).
- [38] V. S. Ptuskin, I. V. Moskalenko, F. C. Jones, A. W. Strong, and V. N. Zirakashvili, “Dissipation of magnetohydrodynamic waves on energetic particles: impact on interstellar turbulence and cosmic ray transport,” *Astrophys. J.* **642** (2006) 902–916, [arXiv:astro-ph/0510335](#).
- [39] G. Jóhannesson *et al.*, “Bayesian analysis of cosmic-ray propagation: evidence against homogeneous diffusion,” *Astrophys. J.* **824** no. 1, (2016) 16, [arXiv:1602.02243](#) [[astro-ph.HE](#)].
- [40] M. J. Boschini *et al.*, “Deciphering the local Interstellar spectra of secondary nuclei with GALPROP/HelMod framework and a hint for primary lithium in cosmic rays,” *Astrophys. J.* **889** (2020) 167, [arXiv:1911.03108](#) [[astro-ph.HE](#)].
- [41] M. J. Boschini *et al.*, “Inference of the Local Interstellar Spectra of Cosmic-Ray Nuclei  $Z \leq 28$  with the GalProp–HelMod Framework,” *Astrophys. J. Suppl.* **250** no. 2, (2020) 27, [arXiv:2006.01337](#) [[astro-ph.HE](#)].
- [42] C. Evoli, D. Gaggero, A. Vittino, G. Di Bernardo, M. Di Mauro, A. Ligorini, P. Ullio, and D. Grasso, “Cosmic-ray propagation with DRAGON2: I. numerical solver and astrophysical ingredients,” *JCAP* **02** (2017) 015, [arXiv:1607.07886](#) [[astro-ph.HE](#)].
- [43] P. Bobik *et al.*, “Systematic Investigation of Solar Modulation of Galactic Protons for Solar Cycle 23 using a Monte Carlo Approach with Particle Drift Effects and Latitudinal Dependence,” *Astrophys. J.* **745** (2012) 132, [arXiv:1110.4315](#) [[astro-ph.SR](#)].
- [44] P. Bobik, M. J. Boschini, S. Della Torre, M. Gervasi, D. Grandi, G. La Vacca, S. Pensotti, M. Putis, P. G. Rancoita, D. Rozza, M. Tacconi, and M. Zannoni, “On the forward-backward-in-time approach for monte carlo solution of parker’s transport equation: One-dimensional case,” *Journal of Geophysical Research: Space Physics* **121** no. 5, (2016) 3920–3930.
- [45] M. J. Boschini, S. Della Torre, M. Gervasi, G. La Vacca, and P. G. Rancoita, “Propagation of cosmic rays in heliosphere: The HELMOD model,” *Adv. Space Res.* **62** (2018) 2859–2879, [arXiv:1704.03733](#) [[astro-ph.SR](#)].
- [46] M. J. Boschini, S. Della Torre, M. Gervasi, G. La Vacca, and P. G. Rancoita, “The HelMod Model in the Works for Inner and Outer Heliosphere: from AMS to Voyager Probes Observations,” *Adv. Space Res.* **64** no. 12, (2019) 2459–2476, [arXiv:1903.07501](#)

[physics.space-ph].

- [47] M. J. Boschini, S. Della, M. Gervasi, G. L. Vacca, and P. G. Rancoita, “Forecasting of cosmic rays intensities with HelMod Model,” *Advances in Space Research* (2022) .
- [48] J. Auffinger and A. Arbey, “Beyond the Standard Model with BlackHawk v2.0,” *PoS CompTools2021* (2022) 017, [arXiv:2207.03266 \[gr-qc\]](#).
- [49] V. De Luca, V. Desjacques, G. Franciolini, A. Malhotra, and A. Riotto, “The initial spin probability distribution of primordial black holes,” *JCAP* **05** (2019) 018, [arXiv:1903.01179 \[astro-ph.CO\]](#).
- [50] T. Chiba and S. Yokoyama, “Spin Distribution of Primordial Black Holes,” *PTEP* **2017** no. 8, (2017) 083E01, [arXiv:1704.06573 \[gr-qc\]](#).
- [51] M. Mirbabayi, A. Gruzinov, and J. Noreña, “Spin of Primordial Black Holes,” *JCAP* **03** (2020) 017, [arXiv:1901.05963 \[astro-ph.CO\]](#).
- [52] T. Harada, C.-M. Yoo, K. Kohri, K.-i. Nakao, and S. Jhingan, “Primordial black hole formation in the matter-dominated phase of the Universe,” *Astrophys. J.* **833** no. 1, (2016) 61, [arXiv:1609.01588 \[astro-ph.CO\]](#).
- [53] T. Harada, C.-M. Yoo, K. Kohri, and K.-I. Nakao, “Spins of primordial black holes formed in the matter-dominated phase of the Universe,” *Phys. Rev. D* **96** no. 8, (2017) 083517, [arXiv:1707.03595 \[gr-qc\]](#). [Erratum: *Phys.Rev.D* 99, 069904 (2019)].
- [54] E. Cotner and A. Kusenko, “Primordial black holes from scalar field evolution in the early universe,” *Phys. Rev. D* **96** no. 10, (2017) 103002, [arXiv:1706.09003 \[astro-ph.CO\]](#).
- [55] S. W. Hawking, “Particle Creation by Black Holes,” in *1st Oxford Conference on Quantum Gravity*. 8, 1975.
- [56] D. N. Page, “Particle Emission Rates from a Black Hole: Massless Particles from an Uncharged, Nonrotating Hole,” *Phys. Rev. D* **13** (1976) 198–206.
- [57] A. Arbey and J. Auffinger, “BlackHawk: A public code for calculating the Hawking evaporation spectra of any black hole distribution,” *Eur. Phys. J. C* **79** no. 8, (2019) 693, [arXiv:1905.04268 \[gr-qc\]](#).
- [58] A. Coogan, L. Morrison, and S. Profumo, “Hazma: A Python Toolkit for Studying Indirect Detection of Sub-GeV Dark Matter,” *JCAP* **01** (2020) 056, [arXiv:1907.11846 \[hep-ph\]](#).
- [59] H. Tashiro and N. Sugiyama, “Constraints on Primordial Black Holes by Distortions of Cosmic Microwave Background,” *Phys. Rev. D* **78** (2008) 023004, [arXiv:0801.3172 \[astro-ph\]](#).
- [60] C. Germani and I. Musco, “Abundance of Primordial Black Holes Depends on the Shape of the Inflationary Power Spectrum,” *Phys. Rev. Lett.* **122** no. 14, (2019) 141302, [arXiv:1805.04087 \[astro-ph.CO\]](#).
- [61] K. Kannike, L. Marzola, M. Raidal, and H. Veermäe, “Single Field Double Inflation and Primordial Black Holes,” *JCAP* **09** (2017) 020, [arXiv:1705.06225 \[astro-ph.CO\]](#).

- [62] B. Carr, M. Raidal, T. Tenkanen, V. Vaskonen, and H. Veermäe, “Primordial black hole constraints for extended mass functions,” *Phys. Rev. D* **96** no. 2, (2017) 023514, [arXiv:1705.05567 \[astro-ph.CO\]](#).
- [63] B. Carr, T. Tenkanen, and V. Vaskonen, “Primordial black holes from inflaton and spectator field perturbations in a matter-dominated era,” *Phys. Rev. D* **96** no. 6, (2017) 063507, [arXiv:1706.03746 \[astro-ph.CO\]](#).
- [64] A. Dolgov and J. Silk, “Baryon isocurvature fluctuations at small scales and baryonic dark matter,” *Phys. Rev. D* **47** (1993) 4244–4255.
- [65] S. Clesse and J. García-Bellido, “Massive Primordial Black Holes from Hybrid Inflation as Dark Matter and the seeds of Galaxies,” *Phys. Rev. D* **92** no. 2, (2015) 023524, [arXiv:1501.07565 \[astro-ph.CO\]](#).
- [66] J. H. MacGibbon and B. R. Webber, “Quark and gluon jet emission from primordial black holes: The instantaneous spectra,” *Phys. Rev. D* **41** (1990) 3052–3079.
- [67] W. Chao, T. Li, and J. Liao, “Connecting Primordial Black Hole to boosted sub-GeV Dark Matter through neutrino,” [arXiv:2108.05608 \[hep-ph\]](#).
- [68] V. S. Berezinsky, S. V. Bulanov, V. A. Dogiel, and V. S. Ptuskin, *Astrophysics of cosmic rays*. 1990.
- [69] A. W. Strong, I. V. Moskalenko, and V. S. Ptuskin, “Cosmic-ray propagation and interactions in the Galaxy,” *Ann. Rev. Nucl. Part. Sci.* **57** (2007) 285–327, [arXiv:astro-ph/0701517](#).
- [70] I. V. Moskalenko and A. W. Strong, “Production and propagation of cosmic ray positrons and electrons,” *Astrophys. J.* **493** (1998) 694–707, [arXiv:astro-ph/9710124](#).
- [71] L. J. Gleeson and W. I. Axford, “Solar Modulation of Galactic Cosmic Rays,” *Astrophys. J.* **154** (1968) 1011.
- [72] M. J. Boschini *et al.*, “Solution of heliospheric propagation: unveiling the local interstellar spectra of cosmic ray species,” *Astrophys. J.* **840** no. 2, (2017) 115, [arXiv:1704.06337 \[astro-ph.HE\]](#).
- [73] M. J. Boschini *et al.*, “HelMod in the works: from direct observations to the local interstellar spectrum of cosmic-ray electrons,” *Astrophys. J.* **854** no. 2, (2018) 94, [arXiv:1801.04059 \[astro-ph.HE\]](#).
- [74] J. F. Navarro, C. S. Frenk, and S. D. M. White, “A Universal density profile from hierarchical clustering,” *Astrophys. J.* **490** (1997) 493–508, [arXiv:astro-ph/9611107](#).
- [75] E. Stone, A. Cummings, and B. Heikkila, “Cosmic ray measurements from voyager 2 as it crossed into interstellar space,” *Nature Astronomy* **3** (11, 2019) .
- [76] **AMS** Collaboration, M. Aguilar *et al.*, “The Alpha Magnetic Spectrometer (AMS) on the international space station: Part II — Results from the first seven years,” *Phys. Rept.* **894** (2021) 1–116.

- [77] M. Simon and U. Heinbach, “Production of anti-protons in interstellar space by propagating cosmic rays under conditions of diffusive reacceleration,” *Astrophys. J.* **456** (1996) 519–524.
- [78] M. Korsmeier and A. Cuoco, “Implications of Lithium to Oxygen AMS-02 spectra on our understanding of cosmic-ray diffusion,” *Phys. Rev. D* **103** no. 10, (2021) 103016, [arXiv:2103.09824 \[astro-ph.HE\]](#).
- [79] Y. Génolini *et al.*, “Cosmic-ray transport from AMS-02 boron to carbon ratio data: Benchmark models and interpretation,” *Phys. Rev. D* **99** no. 12, (2019) 123028, [arXiv:1904.08917 \[astro-ph.HE\]](#).
- [80] L. Orusa, M. Di Mauro, F. Donato, and M. Korsmeier, “New determination of the production cross section for secondary positrons and electrons in the Galaxy,” *Phys. Rev. D* **105** no. 12, (2022) 123021, [arXiv:2203.13143 \[astro-ph.HE\]](#).
- [81] E. Kafexhiu, F. Aharonian, A. M. Taylor, and G. S. Vila, “Parametrization of gamma-ray production cross-sections for pp interactions in a broad proton energy range from the kinematic threshold to PeV energies,” *Phys. Rev. D* **90** no. 12, (2014) 123014, [arXiv:1406.7369 \[astro-ph.HE\]](#).
- [82] T. Kamae, N. Karlsson, T. Mizuno, T. Abe, and T. Koi, “Parameterization of Gamma, e+/- and Neutrino Spectra Produced by p-p Interaction in Astronomical Environment,” *Astrophys. J.* **647** (2006) 692–708, [arXiv:astro-ph/0605581](#). [Erratum: *Astrophys.J.* 662, 779 (2007)].
- [83] P. De la Torre Luque, F. Loparco, and M. N. Mazziotta, “The FLUKA cross sections for cosmic-ray leptons and uncertainties on current positron predictions,” *JCAP* **10** (2023) 011, [arXiv:2305.02958 \[astro-ph.HE\]](#).
- [84] S. Koldobskiy, M. Kachelrieß, A. Lskavyan, A. Neronov, S. Ostapchenko, and D. V. Semikoz, “Energy spectra of secondaries in proton-proton interactions,” *Phys. Rev. D* **104** no. 12, (2021) 123027, [arXiv:2110.00496 \[astro-ph.HE\]](#).
- [85] C. Bierlich *et al.*, “A comprehensive guide to the physics and usage of PYTHIA 8.3,” *SciPost Phys. Codeb.* **2022** (2022) 8, [arXiv:2203.11601 \[hep-ph\]](#).
- [86] M. Di Mauro, F. Donato, M. Korsmeier, S. Manconi, and L. Orusa, “Novel prediction for secondary positrons and electrons in the Galaxy,” *Phys. Rev. D* **108** no. 6, (2023) 063024, [arXiv:2304.01261 \[astro-ph.HE\]](#).